

Association Reactions of Manganese, Iron, and Ruthenium with Nitric Oxide

Roy E. McClean,* Mark L. Campbell, and Michelle D. Vorce

Chemistry Department, United States Naval Academy, Annapolis, Maryland 21402

Laura J. Medhurst

School of Arts and Sciences, Marymount University, Arlington, Virginia 22207

Received: September 28, 1998; In Final Form: January 29, 1999

The gas-phase association reactions of ground-state manganese, iron, and ruthenium atoms with nitric oxide are reported. The transition metal atoms were produced by the 248 nm photodissociation of 2-methylcyclopentadienylmanganese tricarbonyl, ferrocene, and ruthenocene. Detection of these transition metal atoms was by laser-induced fluorescence. Manganese was found to be the least reactive with nitric oxide of the transition metals in this work. The limiting low-pressure third-order rate constant, k_0 , of $\text{Mn} + \text{NO} + \text{Ar}$ can be expressed as $(9.5 \pm 2.5) \times 10^{-33} \exp[-1.5 \pm 0.4 \text{ kcal mol}^{-1}/(RT)] \text{ cm}^6 \text{ molecule}^{-2} \text{ s}^{-1}$. k_0 for $\text{Fe} + \text{NO} + \text{N}_2$ at 296 K is $(2.3 \pm 0.5) \times 10^{-32} \text{ cm}^6 \text{ molecule}^{-2} \text{ s}^{-1}$; this reaction is independent of temperature over the range 296–622 K. Ruthenium was found to be the most reactive toward NO. In Ar buffer, $k_0 = (7.3 \pm 1.0) \times 10^{-30} \text{ cm}^6 \text{ molecule}^{-2} \text{ s}^{-1}$ and the limiting high-pressure rate constant $k_\infty = (3.8 \pm 0.8) \times 10^{-11} \text{ cm}^3 \text{ molecule}^{-1} \text{ s}^{-1}$ for a fixed broadening factor of $F_c = 0.6$. The uncertainties here represent precision. Recent density functional theory calculations on transition metal mononitrosyls were combined with RRKM calculations to estimate the binding energies of the Mn–NO and Fe–NO adducts.

Introduction

The chemistry of gas-phase transition metal (TM) atoms is an attractive field of study because of the relatively large number of low-lying states in many TM atoms. The low-lying states in a particular TM atom may be of different orbital occupancies and hence may exhibit varying degrees of reactivity with a particular reactant. It has been shown that the reaction rates of TM atoms depend, in part, on the orbital occupancy of the TM atom. In particular, states deriving from $d^{n-1}s^1$ electron configurations, where n = number of valence electrons, are generally more reactive than those of $d^{n-2}s^2$ configurations. For example, a survey of dioxygen complexes of 3d TM atoms has shown that TM atoms with singly occupied valence s orbitals are reactive relative to those with doubly occupied valence s orbitals.¹ TM + NO association reactions might follow the same trend. Complex formation of $\text{Fe}(3d^64s^2)$ with NO has been found to be less efficient than complexation of $\text{Cr}(3d^54s^1)$, $\text{Mo}(4d^55s^1)$, $\text{Rh}(4d^85s^1)$, and $\text{Pt}(5d^96s^1)$ with NO.^{2–6} The association reaction of $\text{Re}(5d^56s^2)$ with NO has also been studied.⁷ Even though ground-state Re has a closed s subshell, its reactivity toward NO is comparable to those of Cr, Rh, and Pt. This observation has been discussed in terms of the better size match between the 5d and 6s orbitals compared to the 3d and 4s orbitals.

In this paper, the association reactions of ground-state Mn ($3d^54s^2$), Fe ($3d^64s^2$), and Ru ($4d^75s^1$) with NO are reported. This study not only allows the determination of falloff parameters and barrier effects but it also allows the comparison of the reactivity of TM atoms with different electron configurations. Molecular parameters and binding energies of the mononitrosyls of first-row TM atoms have recently been calculated by density functional theory (DFT) methods.⁸ The DFT calculations predict binding energies of $\sim 50 \text{ kcal mol}^{-1}$ for Mn–NO and Fe–NO. Limiting low-pressure third-order rate constants are very sensi-

tive to binding energies.⁹ If the Mn + NO and Fe + NO reactions proceed with negligible barriers, as observed with many TM + NO reactions, then their reaction rates should be of a comparable order of magnitude. Even though a binding energy is not available for RuNO, the kinetic results can be used to determine if the RuNO adduct is more strongly bound than MnNO and FeNO.

Experimental Section

Details of the experimental arrangement have been described in detail elsewhere¹⁰ and are only summarized here. The laser photolysis/laser-induced fluorescence (LP/LIF) technique was used in this work. The reaction chamber was a stainless steel cross with gas inlet and outlet ports, a viewport for LIF detection, and windows for passage of the laser beams; the chamber was contained in a convection oven capable of attaining temperatures up to 623 K. The TM precursors were methylcyclopentadienylmanganese tricarbonyl (MMT), ferrocene, and ruthenocene. For a given experiment, the precursor was entrained in a flow of buffer gas (argon or nitrogen) and carried to the reaction chamber. For MMT, the carrier gas entrained the MMT and the mixture was then passed through a mass flow controller. The carrier gas passed through a mass flow controller prior to entraining the other two precursors. A slow flow of buffer gas passed over the windows in order to minimize the deposition of the precursor and photofragments. The buffer gas, window gas, and reactant passed through mass flow controllers prior to admission to the reaction chamber. Total flows were between 150 and 8000 sccm, depending on the total pressure. Total flows were varied to test for temperature equilibration and to make sure that the reaction rates did not depend on the overall flow rate. Partial pressures of the individual components were determined by their relative flows and the total pressure in the reaction chamber. Pressures were measured by Baratron

manometers, and temperatures were measured with a thermocouple attached to the reaction chamber.

Fe and Ru were produced from their respective precursors by the focused output of an excimer laser operating on KrF (248 nm) at 21 Hz. The laser beam was unfocused for MMT. Photolysis fluences were between 0.1 and 1 J cm⁻² in the reaction chamber. Detection of the TM atoms was by LIF using laser light from an excimer-pumped dye module. The photolysis and dye beams counterpropagated through the chamber. Neutral density filters were used to ensure that the dye laser fluence did not affect the kinetic results. Dye laser fluences were less than 1 mJ/pulse. Mn(a⁶S_{5/2}) was excited at 403.076 nm, Fe-(a⁵D₄) at 371.994 and 344.061 nm, and Ru(a⁵F₅) at 372.803 nm.^{11–13} Subsequent LIF was detected on resonance using interference filters. A photomultiplier tube and lens focusing system, situated 90° to the laser beams, collected the LIF signal, which was subsequently sent to a gated boxcar sampling module, and the boxcar's output was stored and analyzed by a computer.

All kinetic results are based on the disappearance of the TM atoms under pseudo-first-order conditions where the number density of the TM, [TM], was significantly less than the number density of NO. Reaction time was taken as the delay time between the laser pulses. For a given experimental run, the delay time was varied by a digital delay generator controlled by a computer. Minimum delay times were typically 1–3 μs in order to prevent overlap of the prompt emission with the LIF signal. The trigger source for these experiments was scattered pump laser light incident upon a fast photodiode. LIF decay traces consisted of 200–500 points, each point averaged over 2–10 laser shots. LIF intensities were proportional to TM number densities.

Reagents. The following reagents were used as received: MMT (Aldrich, 97%), ferrocene (Aldrich, 98%), ruthenocene (Aldrich, 97%), Ar (Potomac Airgas, Inc., 99.998%), and N₂ (Potomac Airgas, Inc., 99.998%). Nitric oxide (Liquid Carbonic, 99.0%) had to be purified for the Mn and Fe + NO studies. The NO was passed through a cold trap at about -120 °C prior to passing through the mass flow controller. Since the reactions of Mn and Fe with NO are relatively inefficient, the use of purified NO was important in these systems. The Ru + NO system did not require purified NO.

Data Analysis and Experimental Results

Experiments were generally carried out in the temperature range 295–622 K and in the total pressure range 5–700 Torr. A typical decay plot is presented in Figure 1; the data are for Ru + NO in Ar buffer. Note the growth at relatively short delay times. The growth, attributed to the collisional deactivation of excited states to the ground states, was over in 1–5 μs and had no effect on obtaining the pseudo-first-order rate constant, 1/τ, where τ is the lifetime of the LIF signal. 1/τ is given by

$$1/\tau = 1/\tau_0 + k[\text{NO}] \quad (1)$$

where τ₀ is the lifetime of the TM atom without added nitric oxide. Second-order rate constants, *k*, were obtained from the slopes of plots of 1/τ vs NO pressure such as that shown in Figure 2. Note that the *y* intercept is approximately zero. The *y* intercept, which is equal to 1/τ₀, was relatively small for all experiments and represents the loss of TM atoms from reactions with precursor and photofragments and from diffusion out of the detection zone. The measured second-order rate constants are tabulated in Tables 1–3. The overall uncertainties include statistical scatter, reproducibility in the measured values, and instrumental uncertainties.

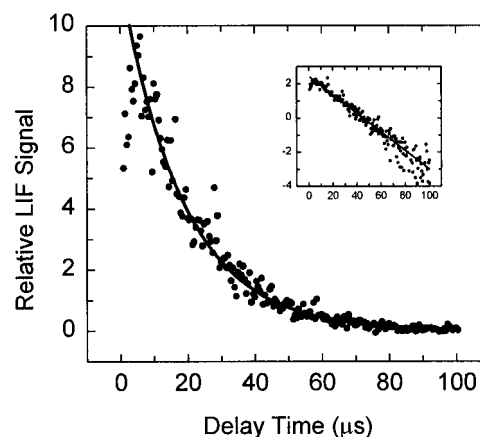


Figure 1. Typical decay profile. Data are for Ru + NO + Ar at 295 K. $P_{\text{NO}} = 181$ mTorr, $P_{\text{total}} = 127$ Torr. The solid line is an exponential fit from which $\tau = 17.2$ μs is obtained. The inset is the same data in the form $\ln(\text{LIF})$ vs time.

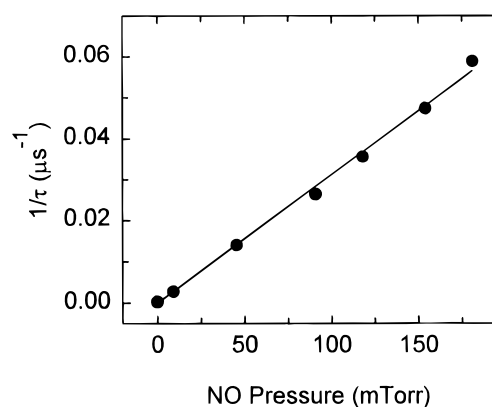


Figure 2. Typical plot for determining the second-order rate constants. Same conditions as those in Figure 1 except for the changing NO pressure. The slope yields $k = (9.65 \pm 0.15) \times 10^{-12}$ cm³ molecule⁻¹ s⁻¹.

TABLE 1: Measured Second-Order Rate Constants for the Reaction Mn(a⁶S_{5/2}) + NO + N₂

P_{total} (Torr)	k (10 ⁻¹⁴ cm ³ molecule ⁻¹ s ⁻¹) ^a			
	295 K	402 K	505 K	622 K
50	0.11		0.19	0.32
100	0.29	0.59	0.34	0.52
200	0.59	0.73	0.74	0.88
300	0.82	1.3	0.99	1.3
400	1.1	1.6	1.7	1.8
500	1.3	1.8	1.8	2.3
600	1.6	2.3	2.5	2.9

^a Uncertainties are ±40% in the 95% confidence limit.

TABLE 2: Measured Second-Order Rate Constants for the Reaction Fe(a⁵D₄) + NO + N₂

P_{total} (Torr)	k (10 ⁻¹⁴ cm ³ molecule ⁻¹ s ⁻¹) ^a		
	296 K	523 K	622 K
20	2.16	1.37	1.26
100	7.36	3.99	3.85
200	12.3	4.12	7.09
300	14.4	11.2	9.37
400	19.2		11.5
500	22.2		13.8
600	24.0		15.6
700	29.3		

^a Uncertainties are ±30% in the 95% confidence limit.

The reaction of Mn with NO was studied predominantly in Ar buffer; a few experiments were performed in N₂ buffer, and rate constants identical to those in Ar buffer were obtained. The rate constants in Table 1 indicate that atomic Mn is very

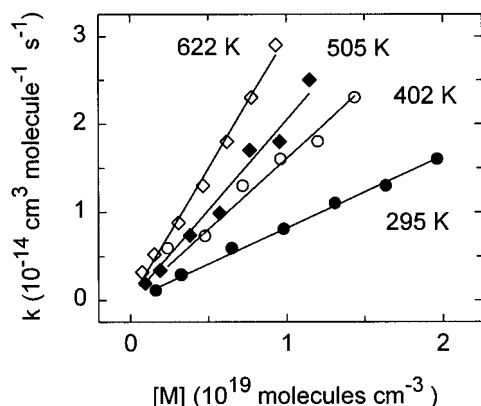


Figure 3. Third-order kinetic behavior of Mn + NO + Ar. The solid lines are linear regression fits from which the third-order rate constants are obtained. See text for results of fit.

TABLE 3: Measured Second-Order Rate Constants for the Reaction Ru(a⁵F₅) + NO + Ar at 295 K

P_{total} (Torr)	k (10^{-12} cm ³ molecule ⁻¹ s ⁻¹) ^a
5	1.20
7.5	1.66
10	1.93
15	2.40
20	2.85
30	4.10
40	4.20
60	6.30
75	7.26
100	8.30
127	9.65
150	11.0
200	13.0
300	15.3
400	19.1
500	20.8
600	24.8
20 (523 K)	0.601

^a Uncertainties are $\pm 25\%$ in the 95% confidence limit.

inefficient in depleting NO. Figure 3 shows the plots of the rate constants as a function of the total number densities, [M]. The solid lines through the data are linear regression fits from which the limiting low-pressure third-order rate constant, k_0 , is obtained. Table 4 lists the results of the fits; note that the third-order rate constants increase with increasing temperature. The third-order rate constants are plotted in Arrhenius form in Figure 4; an activation energy E_a of 1.5 ± 0.4 kcal mol⁻¹ is obtained, where the uncertainty represents $\pm 2\sigma$ precision.

The rate constants for Fe + NO, shown in Table 2, were measured in N₂ buffer. Several rate constants in argon buffer were also measured at 296 K; they were found to be identical, to within experimental uncertainty, to those measured in N₂ buffer at the same temperature. The room-temperature rate constants at 100, 200, and 500 Torr are in agreement with those of Mitchell and Hackett.² Figure 5 shows that the reaction of

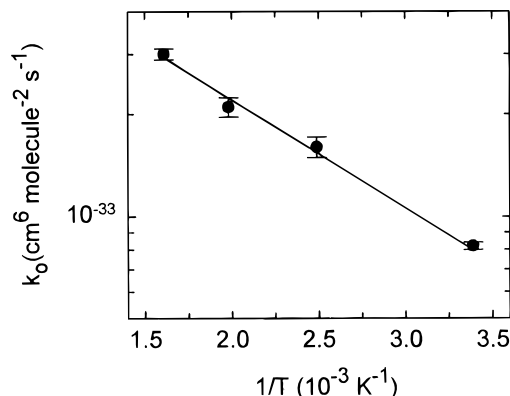


Figure 4. Arrhenius plot of k_0 for Mn + NO + Ar. Error bars represent $\pm 2\sigma$ precision. See text for results of fit.

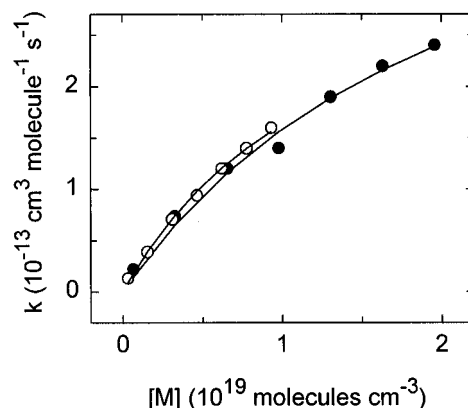


Figure 5. Falloff behavior of Fe + NO + N₂: (●) 296 K; (○) 622 K. The solid lines represent fits to eq 2. See text for results of fit.

Fe with NO does not depend on temperature over the 296–622 K range. The solid lines through the data are fits to the Lindemann–Hinshelwood expression⁹

$$k = \frac{k_0[M]}{1 + k_0[M]/k_\infty} \quad (2)$$

where k_∞ is the limiting high-pressure second-order rate constant. Results of the fits are listed in Table 4. k_∞ is treated as an estimate because of the relatively long extrapolation to the high-pressure limit.

The falloff behavior of Ru + NO in Ar buffer is shown in Figure 6. Ru is more reactive toward NO, and more points are in the falloff region; thus, we were able to use Troe's formalism,¹⁴

$$\log k = \log \left(\frac{k_0[M]}{1 + (k_0[M]/k_\infty)} \right) + \left(\frac{\log F_c}{1 + [\log(k_0[M]/k_\infty)]^2} \right) \quad (3)$$

in obtaining the falloff modeling parameters. F_c is the broadening factor. Relatively large uncertainties for k_∞ and F_c were

TABLE 4: Falloff Modeling Parameters for the Reactions of Mn, Fe, and Ru with NO^a

TM	buffer	T (K)	k_0 (cm ⁶ molecule ⁻² s ⁻¹)	k_∞ (cm ³ molecule ⁻¹ s ⁻¹)	F_c	E_a (kcal mol ⁻¹) ^b
Mn	Ar	295	$(8.2 \pm 0.2) \times 10^{-34}$	$(6.7 \pm 2.9) \times 10^{-13}$	0.6 (fix)	1.5 ± 0.4
		402	$(1.6 \pm 0.1) \times 10^{-33}$			
		505	$(2.1 \pm 0.2) \times 10^{-33}$			
		622	$(3.0 \pm 0.1) \times 10^{-33}$			
Fe	N ₂	296	$(2.3 \pm 0.5) \times 10^{-32}$	$(4.4 \pm 1.1) \times 10^{-13}$	0.6 (fix)	0
		622	$(2.7 \pm 0.3) \times 10^{-32}$			
Ru	Ar	295	$(7.3 \pm 1.0) \times 10^{-30}$	$(3.8 \pm 0.8) \times 10^{-11}$	0.6 (fix)	

^a The uncertainties represent $\pm 2\sigma$ precision. ^b Determined from experimental data.

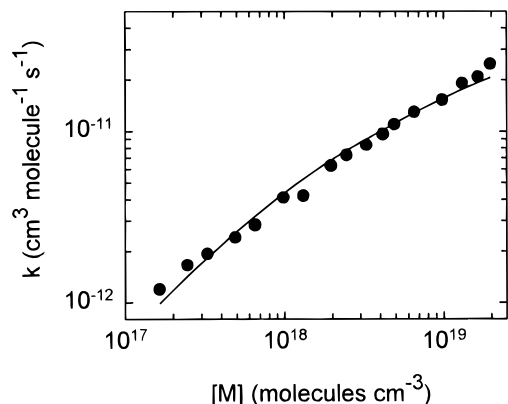
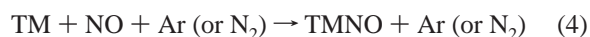


Figure 6. Falloff behavior of Ru + NO + Ar at 295 K. The solid line represents a fit to eq 3, with F_c fixed at 0.6. See text for results of fit.

obtained in the initial fits. Therefore, F_c was fixed at 0.5, 0.6, 0.7, and 0.8. Smaller overall uncertainties were obtained for $F_c = 0.6$. The parameters are listed in Table 4. The reaction rate of Ru with NO in N_2 buffer was found to be identical to that in Ar buffer. Table 3 shows that the rate constant at 523 K and 20 Torr is smaller than the rate constants at 295 K, an indication of no barrier to adduct formation.

Discussion

The results presented above indicate that 1:1 complexes are formed:



Abstraction is not thermodynamically feasible for any of these reactions.^{15,16} The relative values of k_0 of the reactions indicate that Ru($4d^75s^1 a^5F_5$) is the most reactive toward NO followed by Fe($3d^6s^2 a^5D_4$) and then Mn($3d^54s^2 a^6S_{5/2}$). On the basis of the orbital occupancy argument presented above, it is no surprise that Ru is significantly more reactive than Mn and Fe. Any filled s subshell is likely to introduce repulsive effects in the reactions. The first excited state of Mn with an s^1 configuration lies 17052.29 cm^{-1} above the ground state.¹¹ For Fe, the first excited state with an s^1 configuration lies only 6928.280 cm^{-1} above the ground state.¹¹ Thus, the higher reactivity of Fe might be due to the relatively greater accessibility to potential surfaces evolving from s^1 occupancies as reaction proceeds; i.e., mixing between the s^1 and s^2 occupancies may be more probable for Fe. The reactivity of TM ions (TM^+) has also been found to depend on their electron configurations. TM ions with empty valence s orbitals are generally reactive, whereas TM ions with occupied s orbitals are not as reactive.¹⁷ The orbitals that participate strongly in the 3d TM–NO bonding are the 3d and 4s atomic orbitals of the TMs and the 5σ and π^* molecular orbitals of NO.⁸ It seems likely that the d , s , σ , and π^* orbitals will also play dominant roles in the bonding of the 4d TMs such as Ru with NO. The reaction of Mn with NO is characterized by an activation barrier of $1.5 \text{ kcal mol}^{-1}$. Considering the relatively ineffectiveness of this reaction, the barrier is surprisingly small. Mn + NO might proceed entirely on the ground-state surface, which presumably would have a shallow minimum, since k_0 is small. The same possibility exists for the formation of FeNO, which is also inefficient and proceeds with a negligible barrier. The reactions of other TM atoms with NO have also been found to proceed with little or no activation barriers.^{4,18–22} Since the reactions reported here

TABLE 5: Input Parameters for RRKM Calculations^a

	ground-state (quintet) of the MnNO adduct	MnNO transition state
MnNO bond angle	141.41°	141.41°
Mn–N bond length	1.753 Å	3.75 Å
N–O bond length	1.218 Å	1.15 Å
vibrational frequencies	1564 cm^{-1} 551 cm^{-1} 289 cm^{-1}	1903 cm^{-1} 120 cm^{-1}
dissociation energy	20 kcal mol^{-1}	
barrier height	2 kcal mol^{-1}	
collisional energy transfer down	350–400 cm^{-1}	
Leonard-Jones parameters	5.0 Å and 250 K	
	excited state (quartet) of the FeNO adduct	FeNO transition state
FeNO bond angle	140.09°	140.09°
Fe–N bond length	1.688 Å	3.70 Å
N–O bond length	1.205 Å	1.15 Å
vibrational frequencies	1629 cm^{-1} 686 cm^{-1} 252 cm^{-1}	1903 cm^{-1} 60 cm^{-1}
dissociation energy	36 kcal mol^{-1}	
barrier height	1 kcal mol^{-1}	
collisional energy transfer	350 cm^{-1}	
Leonard-Jones parameters	5.0 Å and 250 K	

^a The molecular geometries and frequencies were taken from ref 8.

have small or negligible barriers, the third-order rate constants can be used to determine the relative thermodynamic stabilities of the formed adducts. k_0 is very sensitive to the binding energy, E_b .⁹ Thus, the binding energies fall in the order $E_b(\text{MnNO}) < E_b(\text{FeNO}) < E_b(\text{RuNO})$.

RRKM calculations were performed on the Mn + NO and Fe + NO systems using the UNIMOL program suite of Gilbert et al.²³ The necessary molecular parameters of the adducts were taken from the DFT work of Blanchet et al.⁸ and are listed in Table 5. The Leonard-Jones parameters and the collisional energy transfer down ($\langle E \rangle$) have not been determined experimentally for these systems. However, experimental values of these parameters for several gases are provided in the texts of Gilbert and Smith⁹ and Reid et al.²⁴ On the basis of these tabulations, we chose to estimate these values as presented in Table 5. Similarly, the geometry and vibrational frequencies of the transition states for these systems have not been determined. Thus, we estimated these values as follows. We assumed that the reaction proceeds along the TM–nitrogen bond. The length of this bond was varied from slightly longer than the length in the adduct to 6.0 Å. The length of the N–O bond was also varied from the length in the adduct to the NO molecular bond length. The rotational constants were calculated for each geometry, and the geometry presented in Table 5 gives the best fit to the experimental data. The vibrational frequencies in the transition state were determined by assuming that the TM–N vibration is the degree of freedom that represents the reaction coordinate. For the two remaining vibrations, one was varied between the value of the NO vibration in the adduct and its value in the separated NO molecule, and the other one was allowed to assume any value and was adjusted to fit the data. The values reported in Table 5 for the vibrational frequencies and geometry of the transition state are not necessarily the real values, but they provide the correct density of states at the appropriate temperatures.

Reasonable agreement between calculated and experimental rate constants could not be obtained using the DFT binding

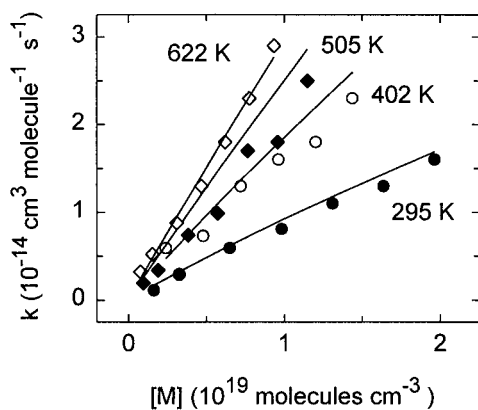


Figure 7. RRKM results for Mn + NO + Ar.

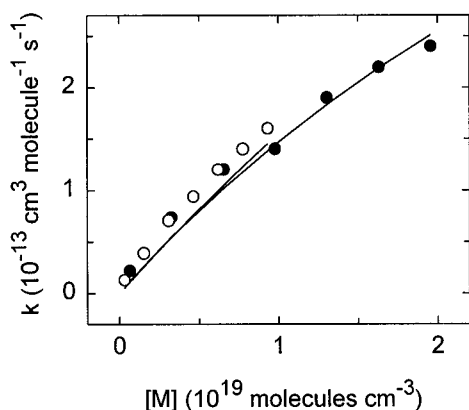


Figure 8. RRKM results for Fe + NO + N₂: (●) 296 K; (○) 622 K.

energies of ~ 50 kcal mol⁻¹ while adjusting the transition-state parameters. Thus, the binding energies were treated as adjustable parameters in the computations. The quintet ground state of MnNO was used as the adduct for the MnNO calculations. Fair agreement between experiment and unimolecular theory was obtained for a binding energy of 20 kcal mol⁻¹ and an energy barrier of 2 kcal mol⁻¹. Since RRKM calculations are only valid on a single potential energy surface, the DFT doublet ground state of FeNO was not used. Instead, the first excited state (quartet) was used in order to conserve spin along the reaction coordinate. Reasonable agreement between the experiment and the RRKM calculations was obtained for a binding energy of 36 kcal mol⁻¹ and an energy barrier of 1 kcal mol⁻¹. Third-order rate constants decrease with increasing temperature for reactions with no activation energy. A zero-temperature dependence over the 296–622 K range suggests a small barrier. Thus, a 1 kcal mol⁻¹ barrier is well within the limits of the experimental and theoretical uncertainties. The RRKM results are presented in Figures 7 and 8. Even though the fits are not perfect, linear behavior is predicted for Mn + NO and falloff behavior is predicted for Fe + NO, as observed.

Summary and Conclusions

The association reactions of Mn, Fe, and Ru with NO have been investigated as a function of temperature and pressure. These reactions exhibited little or no activation barriers. The relative reactivity of these TM atoms falls in the order Mn < Fe < Ru. Results are interpreted in terms of the orbital occupancies of the TMs; i.e., TMs with an s¹ configuration such as Ru are generally more reactive than TMs with s² configurations such as Fe and Mn. Recent density functional theory calculations on transition metal mononitrosyls were combined with RRKM calculations to estimate the binding energies of the Mn–NO and Fe–NO adducts: $E_b(\text{Mn–NO}) = 20$ kcal mol⁻¹; $E_b(\text{Fe–NO}) = 36$ kcal mol⁻¹. A binding energy for Ru–NO > 36 kcal mol⁻¹ is inferred from the relatively large third-order rate constant.

Acknowledgment. This research was supported by the Naval Academy Research Council and a Cottrell College Science Award of Research Corporation.

References and Notes

- (1) Brown, C. E.; Mitchell, S. A.; Hackett, P. A. *J. Phys. Chem.* **1991**, *95*, 1062.
- (2) Mitchell, S. A.; Hackett, P. A. *J. Chem. Phys.* **1990**, *93*, 7822.
- (3) Parnis, J. M.; Mitchell, S. A.; Hackett, P. A. *J. Phys. Chem.* **1990**, *94*, 8152.
- (4) McClean, R. E.; Campbell, M. L.; Goodwin, R. H. *J. Phys. Chem.* **1996**, *100*, 7502.
- (5) Campbell, M. L. *Laser Chem.* **1998**, *17*, 219.
- (6) Campbell, M. L. *J. Chem. Soc., Faraday Trans.* **1998**, *94*, 353.
- (7) Campbell, M. L. *J. Phys. Chem.* **1998**, *102*, 892.
- (8) Blanchet, C.; Duarte, H. A.; Salahub, D. R. *J. Chem. Phys.* **1997**, *106*, 8778.
- (9) Gilbert, R. G.; Smith, S. C. *Theory of Unimolecular and Recombination Reactions*; Blackwell Scientific Publications: Boston, 1990.
- (10) Campbell, M. L.; McClean, R. E. *J. Chem. Soc., Faraday Trans.* **1995**, *91*, 3787.
- (11) Moore, C. E. Atomic Energy Levels as Derived from the Analysis of Optical Spectra. *Natl. Stand. Ref. Data Ser. (U.S., Natl. Bur. Stand.)* **1971**, NSRDS-NBS 35.
- (12) Martin, G. A.; Fuhr, J. R.; Wiese, W. L. *J. Phys. Chem. Ref. Data* **1988**, *17* (Suppl. 3 and 4).
- (13) Meggers, W. F.; Corliss, C. H.; Scribner, B. F. Tables of Spectral-Line Intensities, Part I: Arranged by Elements. *Natl. Bur. Stand., Monogr. (U.S.)* **1975**, 145.
- (14) Troe, J. *J. Phys. Chem.* **1979**, *83*, 114.
- (15) Chase, M. W., Jr.; Davies, C. A.; Downey, J. R., Jr.; Frurip, D. J.; McDonald, R. A.; Syverud, A. N., Eds. JANAF Thermochemical Tables, 3rd ed. *J. Phys. Chem. Ref. Data* **1985**, *14* (Suppl. 1).
- (16) Lide, D. R., Ed. *CRC Handbook of Chemistry and Physics*, 75th ed.; CRC Press: Boca Raton, FL, 1995.
- (17) Armentrout, P. B. *Science* **1991**, *251*, 175.
- (18) McClean, R. E.; Pasternack, L. *J. Phys. Chem.* **1992**, *96*, 9828.
- (19) McClean, R. E.; Campbell, M. L.; Kolsch, E. J. *J. Phys. Chem. A* **1997**, *101*, 3348.
- (20) Campbell, M. L.; McClean, R. E. *J. Phys. Chem.* **1993**, *97*, 7942.
- (21) Campbell, M. L.; Hooper, K. L. *J. Chem. Soc., Faraday Trans.* **1997**, *93*, 2139.
- (22) Harter, J. S. S.; Campbell, M. L.; McClean, R. E. *Int. J. Chem. Kinet.* **1997**, *29*, 367.
- (23) Gilbert, R. G.; Smith, S. C.; Jordan, M. J. T. *UNIMOL Program Suite*; School of Chemistry, Sydney University: Australia, 1993.
- (24) Reid, R. C.; Prausnitz, J. M.; Poling, B. E. *The Properties of Gases & Liquids*, 4th ed.; McGraw-Hill Book Company: New York, 1987.